Effect of Fragmenting Buried High Explosive Projectile (152mm HE Frag OF-540) on Military Ground Vehicles

Venkatesh Babu, Sanjay Kankanalapalli, Madanmohan Vunnam

U.S. Army - Combat Capabilities Development Command (CCDC),
Ground Vehicle System Center (GVSC) – Survivability & Protection M&S Team,
Warren, MI 48397, USA

Abstract

Simulation of Military ground vehicles subjected to buried landmines, and Improvised Explosive Devices (IED) has been carried out by many researchers, and military establishments to understand the effects in detail. But the ability to predict the effects of fragmenting IED's on military ground vehicles is little known in simulation community. Hydrocode simulation such as Eulerian simulation and Arbitrary Lagrange in Eulerian (ALE) simulation coupled to vehicle structure is widely used methodology to characterize buried detonating IED. Fragmentation is the breakage of a body into several small pieces due to mechanical loadings. Dynamic fragmentation process between ductile materials and brittle materials goes through three phases: crack nucleation, crack propagation and fragmentation. Density and strength of materials dictates the phases of dynamic fragmentation. Fragments of different shape and size are formed when cracks coalesce. Understanding this process is crucial in estimating the number of fragments, size and its effect on impacting structures. There are several statistical and empirical formulations that are available to approximately estimate the number of fragments, but does not provide sufficient information about the velocities of the fragments. For military ground vehicles it is essential to know and understand not only the size of the fragments but also its velocities and secondary damages it can cause on the vehicle hull. In this proposed study, a 152mm High Explosive (HE) OF-540 fragmenting projectile was modelled in detail per geometry and buried 100 mm deep inside the soil. This fragmenting projectile was coupled to U.S. Army's Ground Vehicle System Center (GVSC) developed generic hull (GH) structure to understand the impact effects of fragmenting fragments. Three different analysis were carried out Projectile buried in soil with adaptive SPH projectile casing, Projectile buried in soil coupled to GH structure with projectile casing as ALE and projectile casing as adaptive SPH methods. Results from all the three analysis were thoroughly analyzed and findings from these analysis is presented in this paper. Solid element formulation is well suited for shock waves, crack propagation and fragmentation problems was used in modeling all the structural and projectile components using commercially available structural code LS-DYNA-3D.

Keywords: *Improvised Explosive Device, fragments, discrete particles, adaptive SPH, erosion*

1.0 Introduction

Military ground vehicles are exposed to wide variety of threats in theaters such as buried mines, fragmenting IED, magnetically attached IED, Projectiles and other kinetic energy threats. Most of these threats carries high explosives housed in metal casings. When these HE detonates resulting high pressure expands the metal casings and eventually ruptures and travels with very high velocities. Expanding pressure wave and the fragmented metal parts impacts the military vehicles and causes damages from minimal to catastrophic depending on the size of the charge. Soldiers inside the vehicles are subjected to very high accelerative and impulse loading [1]. Several blast mitigating technologies are developed and inserted to minimize the structural damages and soldier injuries such as V-Hull, Stroking floors and seats. Most often these are developed for objective and threshold threat levels and if the threat exceeds these limits, damages are far more.

Hand calculations and empirical formulas are not suitable for highly non-linear problems of HE explosions, shock loading and fragmentation. Limited set of experimental data are available to develop empirical formulas. However for most of the HE explosions, problems are analyzed by complex analytical technique, generally computational solvers. Experimental tests are crucial in development of computational models, without which computational models become unreliable.

Fragmentation is breaking a continuous body into several small pieces. Several researchers namely Rosin-Rammler [1933], Weibull [1939], N.F. Mott [1947], Linfoot [1943], Gilvarry [1961], Grady [1982, 2007] and many others have performed numerous expanding ring and cylinder experiments to study the fragmentation process in detail and developed several mathematical and statistical theories. [2-8]. In this paper, fragmenting 152mm OF-540 projectile was analyzed using ALE and ADAPTIVE SPH TO SOLID methods using commercially available LS-DYNA [9] non-linear solver from an application point of view. Main objective of this paper was to capture the fragmentation process computationally by Eulerian and Lagrangian with adaptive SPH methods and its effect of on the military ground vehicle structures and compare the selected responses.

2.0 FEM Model of 152mm OF-540

Hypermesh pre-processor was used to mesh the OF-540 using the CAD geometry. Several models were created from 1 mm element size to 5 mm element size to understand the process of fragmentation and element erosion.

2.1 OF-540 model

OF-540 is a fragmenting 152mm diameter projectile. Specification of the OF-540 shown in figure 1. Diameter of the charge varies from 31 mm near the fuse to 104 mm at the center. Metal casing also has varying thickness across the length of the explosive from 20 mm near the fuse to 31 mm at the far end of the fuse. Total length of the threat is 641 mm. piezoelectric fuse is 33 mm in diameter and 35 mm in length. 8 node solid elements were used to mesh the OF-540 model. Although 4 noded shell element is easier and faster, but not recommended for blast and fragmentation problems. Meshed OF-540 model shown next to the specification has over 3 million solid elements. HE inside the projectile casing is represented as Eulerian and casing as

Lagrange with adaptive SPH. There are several meshless method options such as DEM [10] and SPG, are emerging, but SPH is widely used.

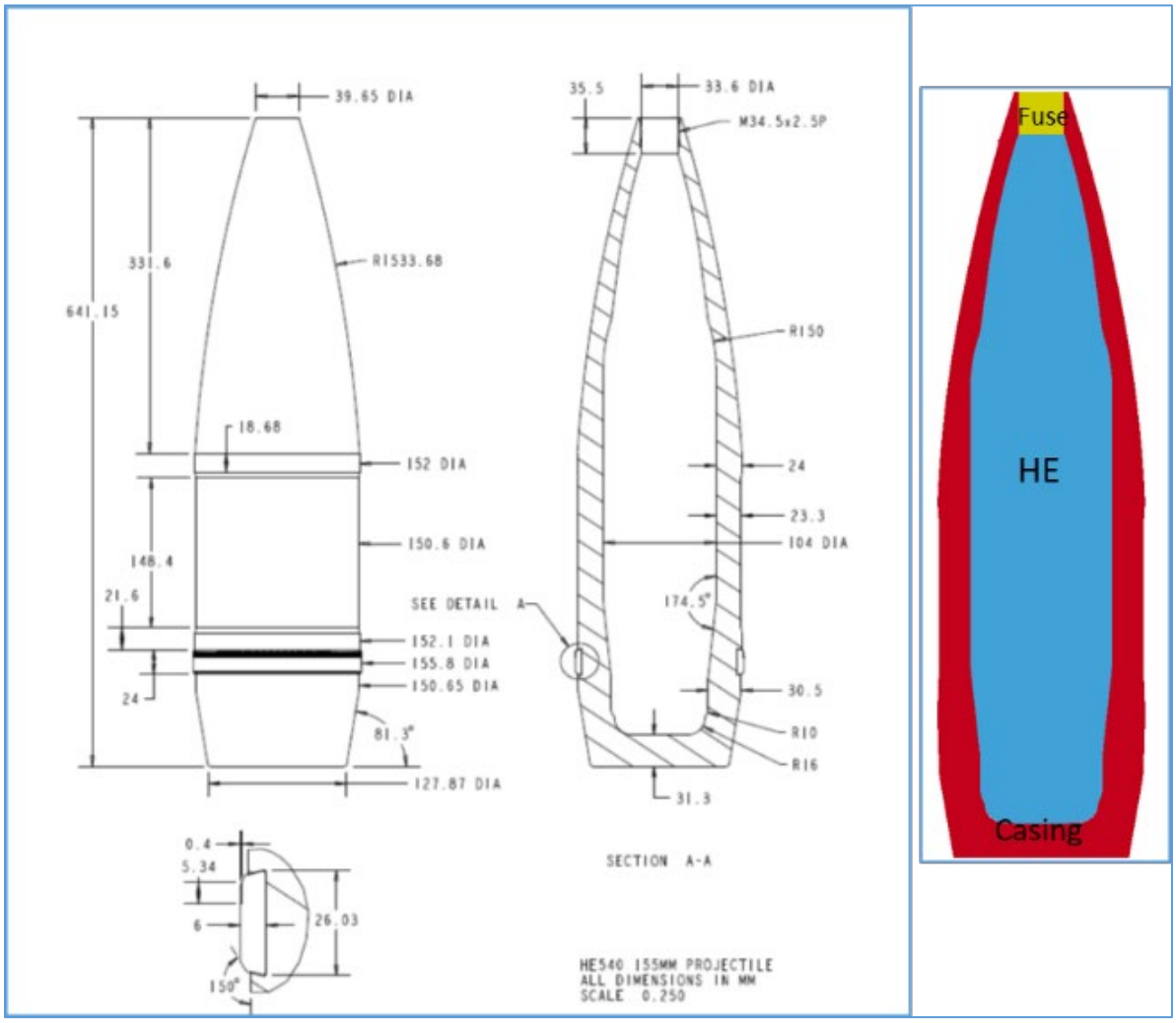

Figure 1: Geometry and Specification of OF-540

2.2 GVSC Generic Hull Model

Generally most of the blast events are classified in nature. This limits the accessibility of the data for research community in academia and industry partners to develop any meaningful mitigating strategies. To alleviate this, CCDC GVSC developed a generic hull (GH) structure. This GH was subjected to blast loading and the data generated can be shared with academia researchers and industry partners to collaborate and develop different blast mitigating technologies and simulation methods. Picture of GH model is shown in figure 2 has 786,000 solid elements.

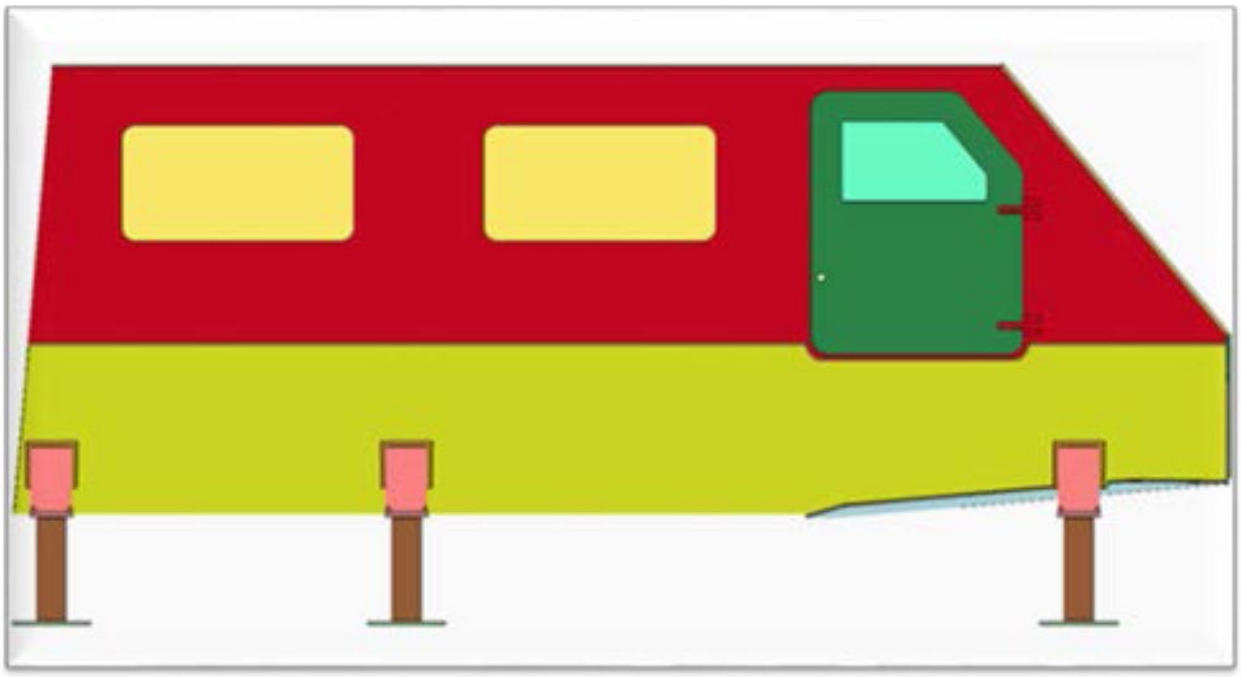

Figure 2. GVSC Generic Hull Structure

2.3 Material Models

Materials used in ALE, OF-540 and GH structure are shown in LS-DYNA format

ALE Materials

HE – TNT

```
*MAT_HIGH_EXPLOSIVE_BURN
$      mid        ro         d          pcj        beta         k          g        sigy
        31    1590.0    6741.0    2.60E+10       0.000       0.000      0.000      0.000
*EOS_JWL
$    eosid          a          b          r1          r2       omega         e0         vo
        31 3.71E+11   3.23E+9     4.1500      0.9500      0.3000  6.2E+9     1.0000
```

Soil

```
*MAT_ELASTIC_PLASTIC_HYDRO_SPALL
$  (12.0% AFV content)
$#        mid         ro          g       sigy         eh         pc         fs      charl
          11   1908.937  7.78E+7   2.700+7   1.000+6   -6900.00      0.000      0.000
$#         a1         a2      spall
       0.000      0.000      2.000
$#       eps1       eps2       eps3       eps4       eps5       eps6       eps7       eps8
       0.000      0.000      0.000      0.000      0.000      0.000      0.000      0.000
$#       eps9      eps10      eps11      eps12      eps13      eps14      eps15      eps16
```

```
        0.000       0.000       0.000       0.000       0.000       0.000       0.000       0.000
*EOS_TABULATED_COMPACTION
$ Soil as adjusted (12.0% AFV content)
$ ---------- + ---------- + ---------- + ---------- + ---------- + --------- + --------- + --------- +
$#      eosid      gamma         e0          vo
             11      0.000      0.000        1.00
$ ----------+ ---------- + ---------- + ---------- + ---------- +
$#         ev1         ev2         ev3         ev4         ev5
       0.0000   -0.064539     0.07985   0.095161   -0.138785
,,,,,,
,,,,,,
```

Air

```
*MAT_NULL
$         mid        ro        pc        mu       terod      cerod      ym         pr
              32   1.2985       0.0 1.8444E-5       0.0        0.0        0.0        0.0
```

```
*EOS_LINEAR_POLYNOMIAL
$         eosid        c0         c1         c2         c3         c4         c5         c6
              32     0.000      0.000      0.000      0.000     0.4000     0.4000     0.000
$              e0         v0
   2.533125E5        1.0
```

OF-540 Material

```
*MAT_JOHNSON_COOK_TITLE
OF- 540
$#        mid         ro          g          e         pr        dtf        vp       rateop
             540    7830.00  7.75E+9 2.11E+11       0.30      0.000      1.00       0.00
$#          a           b          n          c         m         tm         tr       epso
      6.18E+8     6.990+8     0.3500  0.02060     1.0300  1793.00    291.00       1.00
$#         cp          pc       spall         it        d1        d2         d3        d4
         477.00  -5.270E+9         1.0       1.00      0.100   0.3020     -0.7853   0.0168
$#         d5          c2/p       erod      efmin

          0.8260         0.00          0     1.00E-6
```

```
*EOS_GRUNEISEN_TITLE

OF-540
$#         eosid         c          s1         s2         s3        gamao         a          e0
              54  4578.00    1.3300       0.00       0.00       1.6700     0.4300       0.00
$#            v0
          1.0000
```

GH Structure modeled with Johnson-Cook strength and failure model [11]

```
*MAT_JOHNSON_COOK_TITLE
RHA
$#      mid        ro         g         e        pr       dtf        vp     rateop
          1    7850.0  7.960E10 2.068E11      0.27       0.0       1.0       0.0
$#        a         b         n         c         m        tm        tr      epso
 7.9220E8  5.0950E8      0.26     0.014      1.03    1818.0     300.0       1.0
$#       cp        pc     spall        it        d1        d2        d3        d4
      448.0   -6.90010       2.0       1.0      -0.8       2.1       0.5     0.002
$#       d5      c2/p      erod     efmin
       0.61       0.0         0  1.00E-6
```

```
*EOS_GRUNEISEN_TITLE
RHA
$#     eosid         c        s1        s2        s3     gamao         a        e0
          1    4578.0      1.33       0.0       0.0       1.67      0.43       0.0
$#       v0
       1.0
```

3.0 Analysis Matrix

Analysis was performed with and without structure for OF-540 threat. Five sets of analysis were performed:

1. OF-540 buried 100mm in soil, without structure coupling – adaptive SPH casing
2. OF-540 Surface laid, coupled to GH structure - adaptive SPH casing
3. OF-540 Buried 100mm in soil, ALE FSI coupling, - Eulerian casing
4. OF-540 Buried 100 mm in soil, ALE FSI coupling with Lagrange casing
5. OF-540 Buried 100 mm in soil, ALE FSI coupling with adaptive SPH casing

First OF-540 was evaluated without any structure coupling to make sure that detonation process and fragmentation are free of numerical instabilities and smooth. Second analysis was performed with OF-540 laid on ground surface and coupled to GH structure. In this analysis momentum effect of soil will be minimal on the GH structure. In the third analysis OF-540 was buried 100 mm deep inside the soil and detonated. Here OF-540 was modeled as ALE. Explosive was modeled as Eulerian in all the analysis. In this particular analysis metal casing over explosive is also modeled as Eulerian and used LS-DYNA ALE multi-material coupling. In the fourth analysis metal casing over explosive was modeled as Lagrangian. In the fifth analysis in addition to modeling metal casing over explosive as Lagrangian, ADAPTIVE_SOLID_TO_SPH was invoked to convert the failed metal casing parts into smooth particles.

3.1 Without Structure

OF-540 threat buried 100 mm deep inside the soil is shown in figure 2. Charge was detonated and fragmentation process was captured. Sequence of detonation is captured in figure 3 from detonation time to complete fragmentation process.

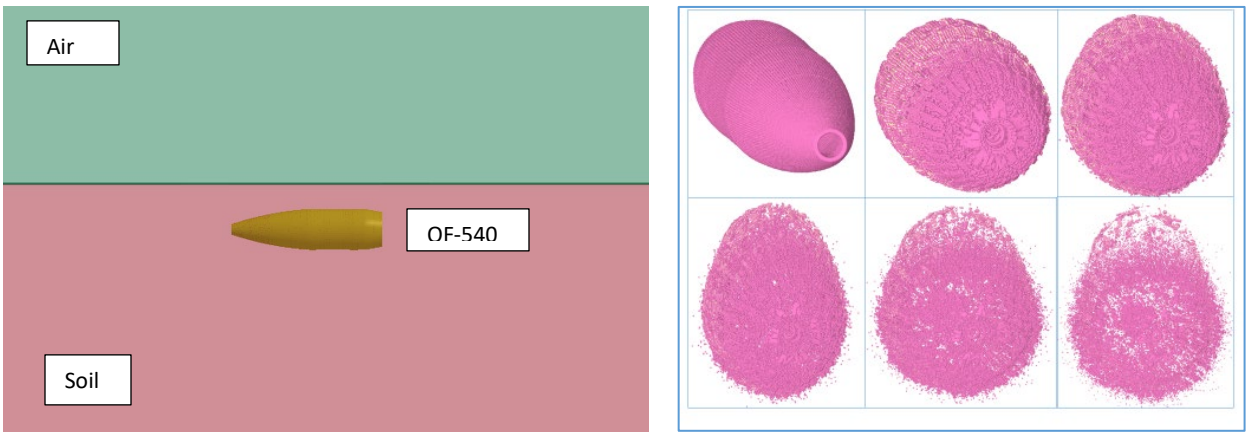

Figure 2. Buried OF-540 without structure

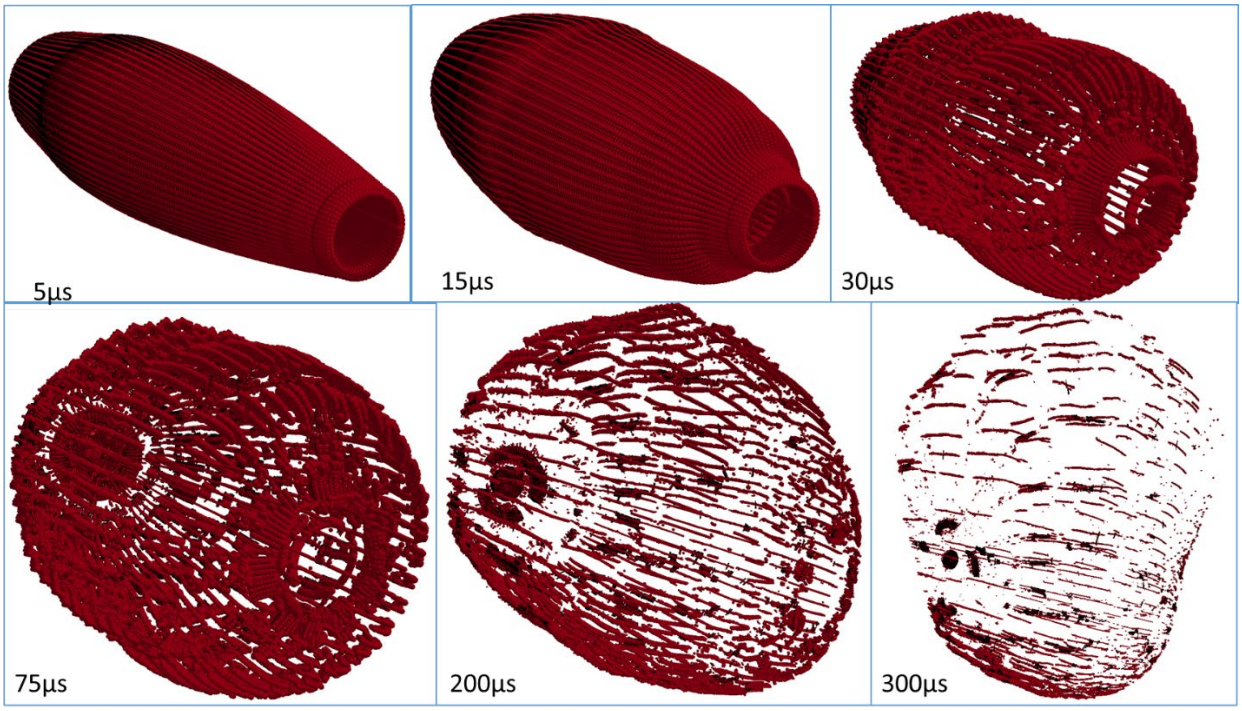

Figure 3. Buried OF-540 without structure

Crater formation of 1.6 meter in length and 1.5 meter in depth will be formed as shown in figure 4.

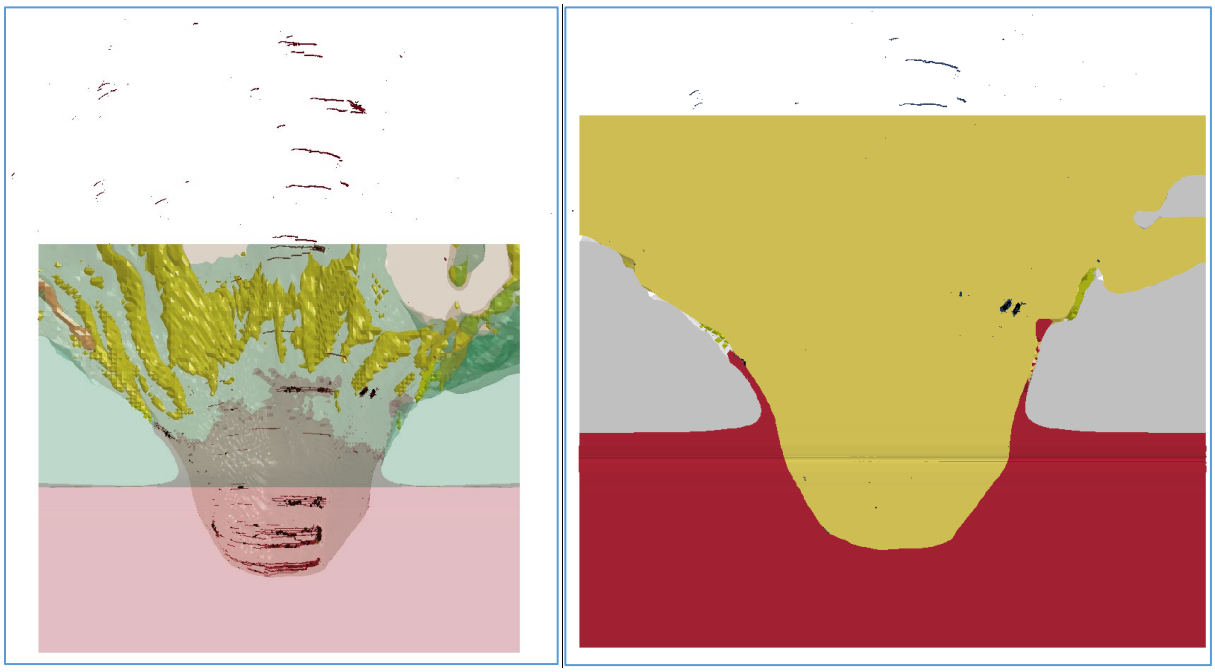

Figure 4. Crater formation without structure

3.2 With GVSC GH structure

After establishing high confidence in the detonation and fragmentation process, next step was to couple the OF-540 to GVSC GH structure. All the set-up remains same as described in section 3.1 with GH structure coupled as shown in figure 5. Location of the charge was close to the center of the structure between front and mid-point legs.

Two contacts need to be defined, one between the multi-material fluid particles to the structure and another one between the adaptive SPH particles to the structure. Contact between the structure and the HE charge is activated via *CONSTRAINED LAGRANGE IN SOLID (CLIS). And contact between the SPH particles to the structure is defined via CONTACT AUTOMATIC NODES TO SURFACE. Details on how to use these cards is available in LS-DYNA user's manual [9]

```
*CONSTRAINED_LAGRANGE_IN_SOLID
$#     slave    master     sstyp     mstyp     nquad     ctype     direc     mcoup
       1240      1111         0         0         2         5                  -12
$#     start       end      pfac      fric    frcmin      norm   normtyp      damp
 0.000E+00     0.060     0.200      0.00   0.25000                            0.00
$$#     cq      hmin      hmax     ileak     pleak    lcidpor     nvent  blockage
                                       2      0.15
```

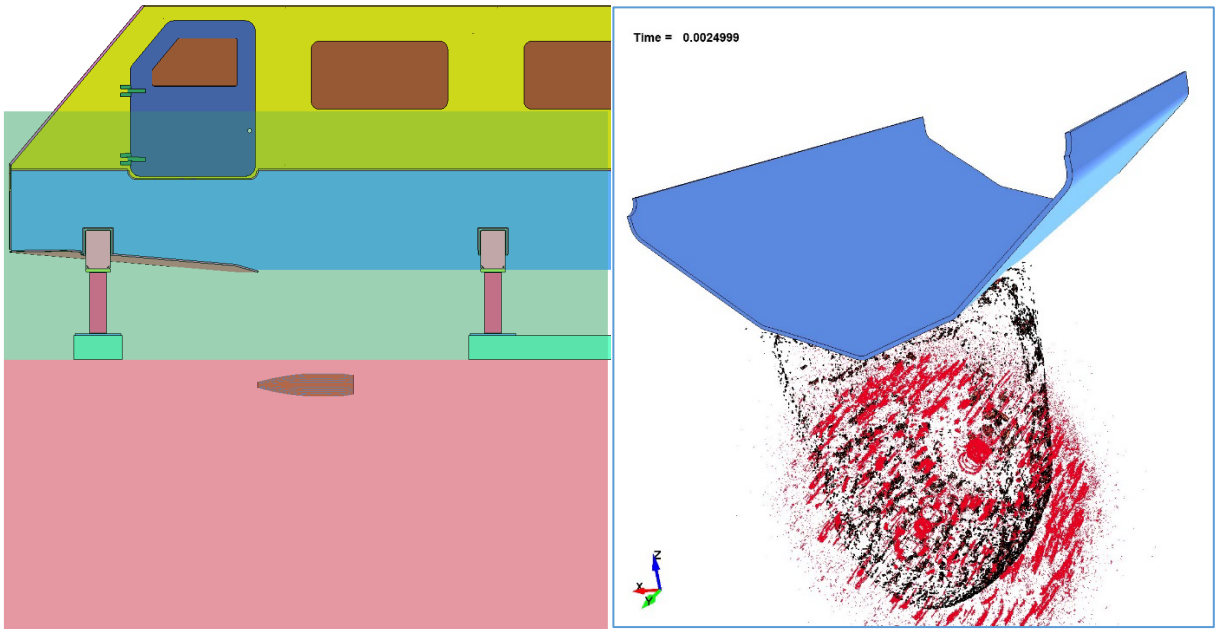

Figure 5. OF-540 coupled to GH structure

Fragmented particles and debris are shown in figure 5 for buried HE and figure 6 shows the sequence of fragmentation process coupled to the GH structure for surface laid HE.

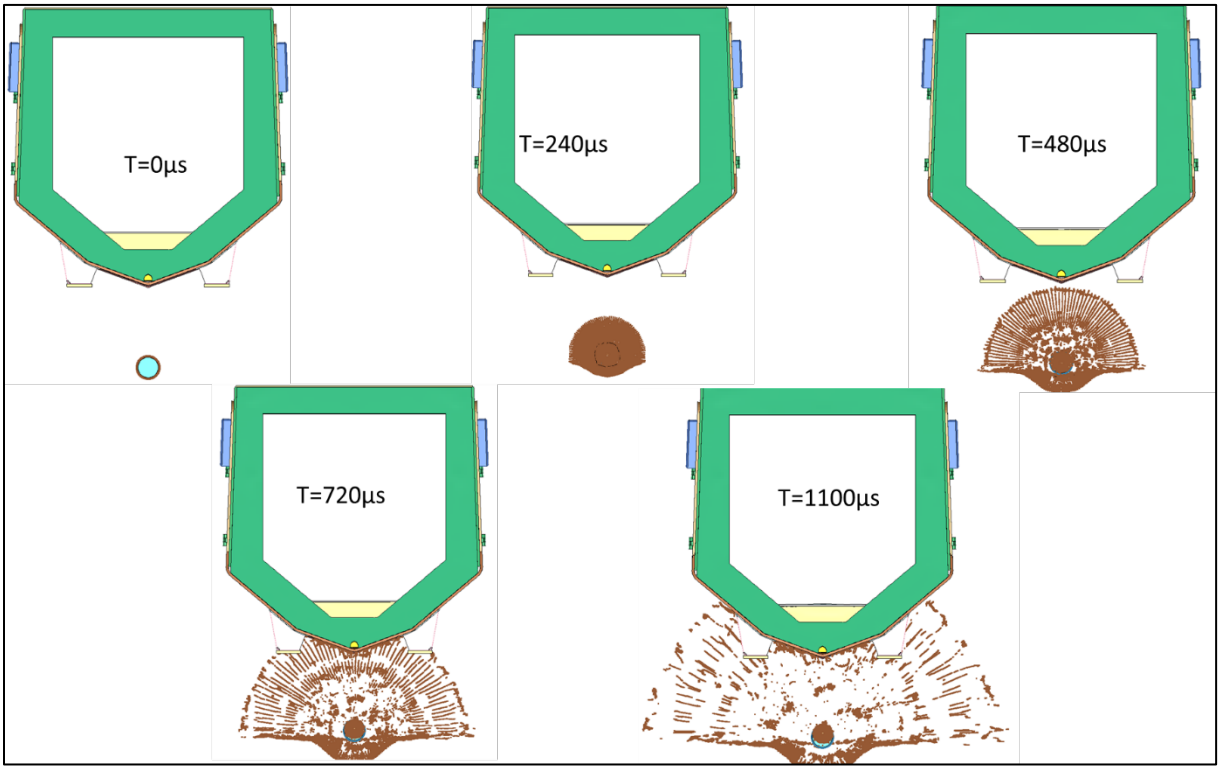

Figure 6. Sequence of fragmentation and coupling to GH structure – Surface laid HE

4.0 Results and Discussion

4.1 Loss of mass

When projectile casing modeled as Lagrange or Eulerian, casing loses mass significantly due to erosion. This will maintain the numerical stability and continue the analysis till the termination time. This results in inaccurate conservation mass, momentum and energies. In order to eliminate the loss of mass, projectile casing was also modeled with adaptive SPH particles. By invoking adaptive SPH, failed Lagrange elements were converted into SPH particles and these particles carry the mass momentum and energy. Figure 7 shows the mass of projectile casing in time domain

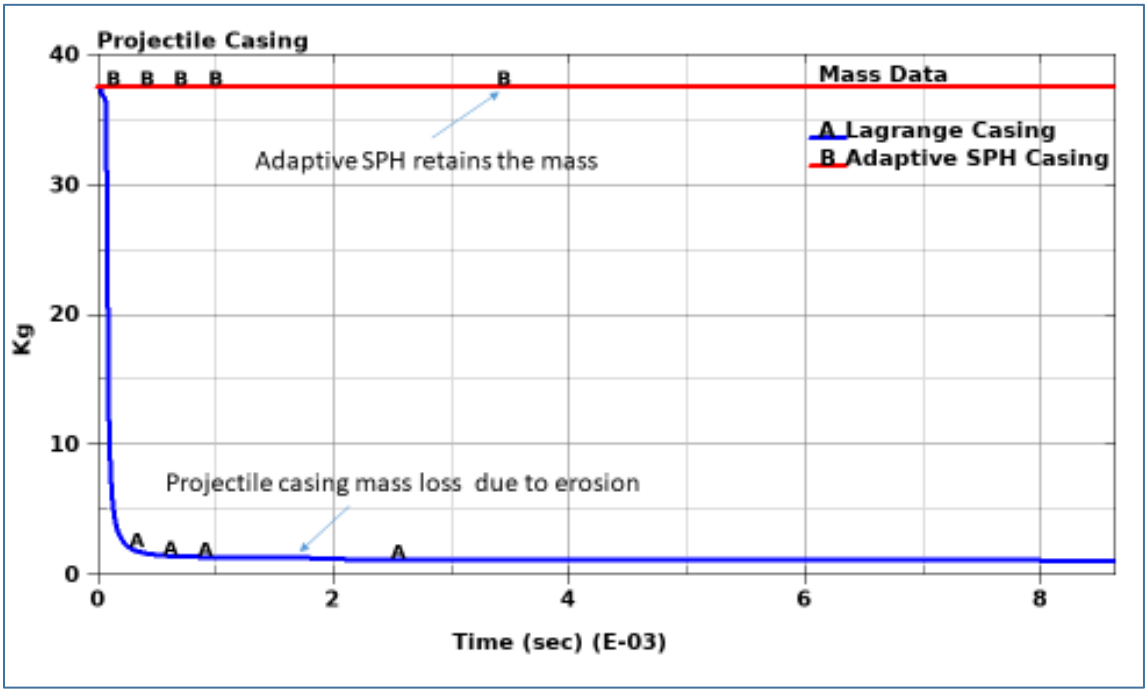

Figure 7: Projectile casing mass

To determine whether this mass loss is sensitive to element size, projectile was modeled with 2 mm and 1 mm elements sizes. Loss of mass trend did not change for finer element sizes. Table 1 shows the data from 3 mm and 1 mm element size projectiles. Figure 8 is the curve generated from table 1.

Table 1: Lost mass from OF-540 Fragmentation

Lost mass from OF-540 Projectile Casing				
	Coarse		Fine	
Time (sec)	Mass	% Coarse	Mass	%Fine

0	37.61	0	37.61	0
0.00005	36.8	2.153683	36.87	1.967562
0.00012	3.96	87.3172	6.99	79.44696
0.00016	2.97	92.10316	3.83	89.81654
0.00038	1.91	94.92156	1.64	95.63946
0.00077	1.62	95.69263	0.34	99.09599
0.001	1.52	95.95852	1.27	96.62324
0.002	1.245	96.68971	1.18	96.86254
0.003	1.147	96.95028	1.11	97.04866
0.007	1.067	97.16299	1.08	97.12842

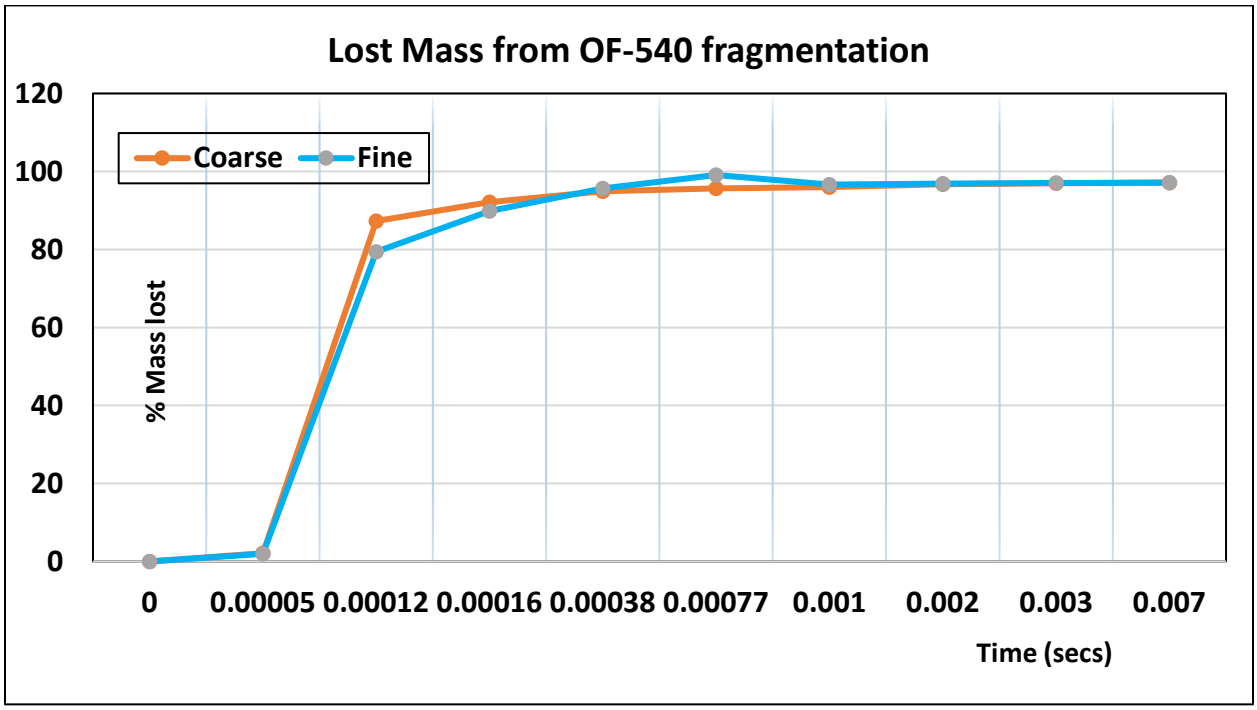

Figure 8: Projectile casing mass loss

It is clear from table 1 and figure 8, 80% of the projectile casing mass will be lost within 120 microseconds of detonation. Loss of mass at different time intervals are captured in figure 9.

Projectile casing starts to expand immediately after the detonation of high explosive charge (TNT in this case) inside the casing. High pressure generated by the shock wave of the detonating products results in volume expansion. Combination of expanding volume and high pressure on the inside surface of the projectile casing generates high stresses and high strains on the metal surfaces, resulting in rupture and shearing of the casing. These ruptured materials

(fragments) fly in directions depending upon the geometry, thickness, velocity and rejection angle.

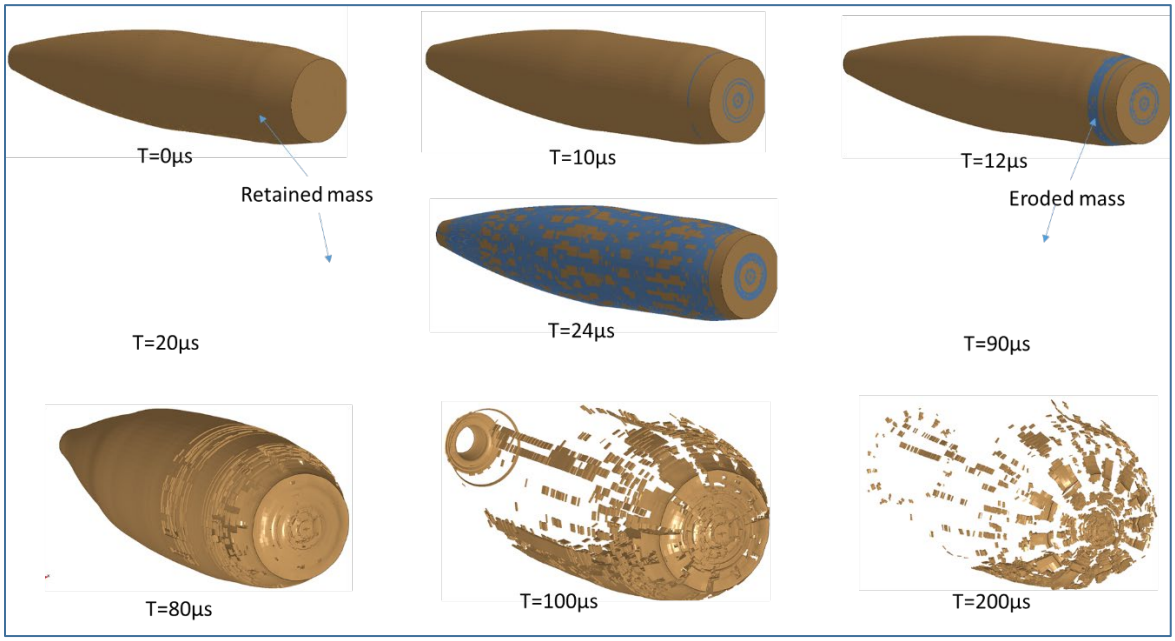

Figure 9: Projectile casing mass loss at different time intervals

4.2 Fragment velocities

Fragment velocities are higher for surface laid HE than that of the buried HE. This can be attributed to absence of soil resistance for fragments. Velocity-time response is shown in figure 10 for surface laid HE and figure 11 for buried HE along with sensor locations. Fragments near the detonation location travels at speed over 1000 m/s and away from the detonation location travels at a speed of 600 m/s for surface laid HE. Whereas, fragment velocities are under 500 m/s for buried HE. In case of buried HE, fragment velocities are damped by the presence of soil and fragments have to overcome the soil pressure. Smaller the size of the fragments higher the velocity and larger the fragment size lower the velocity. Even though smaller fragments size travels at higher speed with lower mass, its ability to make a meaningful impact on the target is relatively lower compared to that of the larger fragments with higher mass.

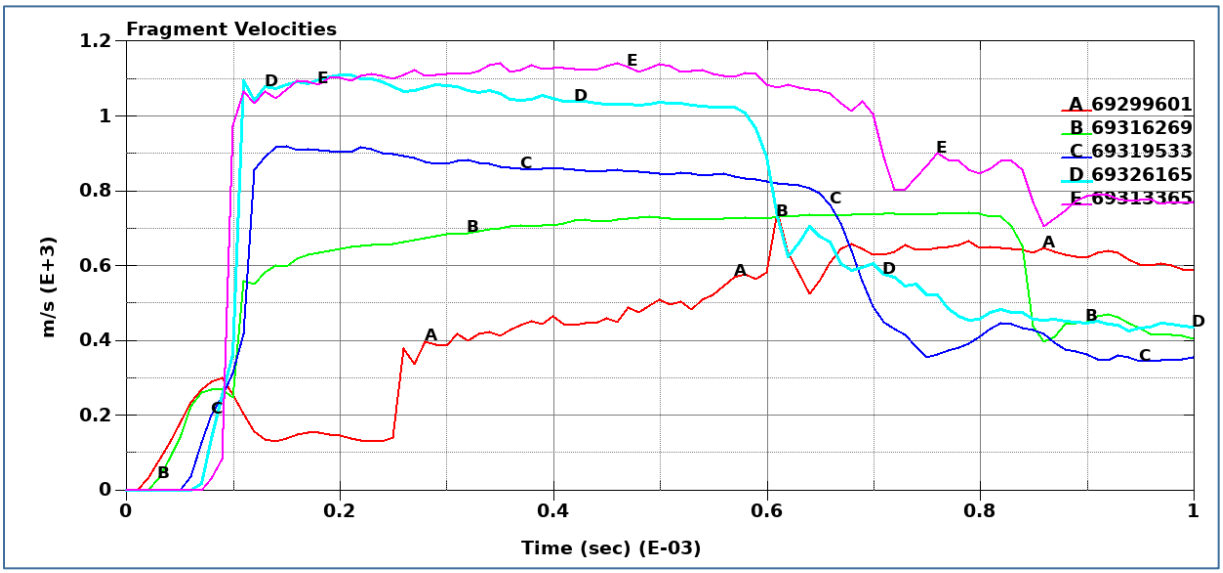

Figure 10: Fragment velocity: Surface Laid HE

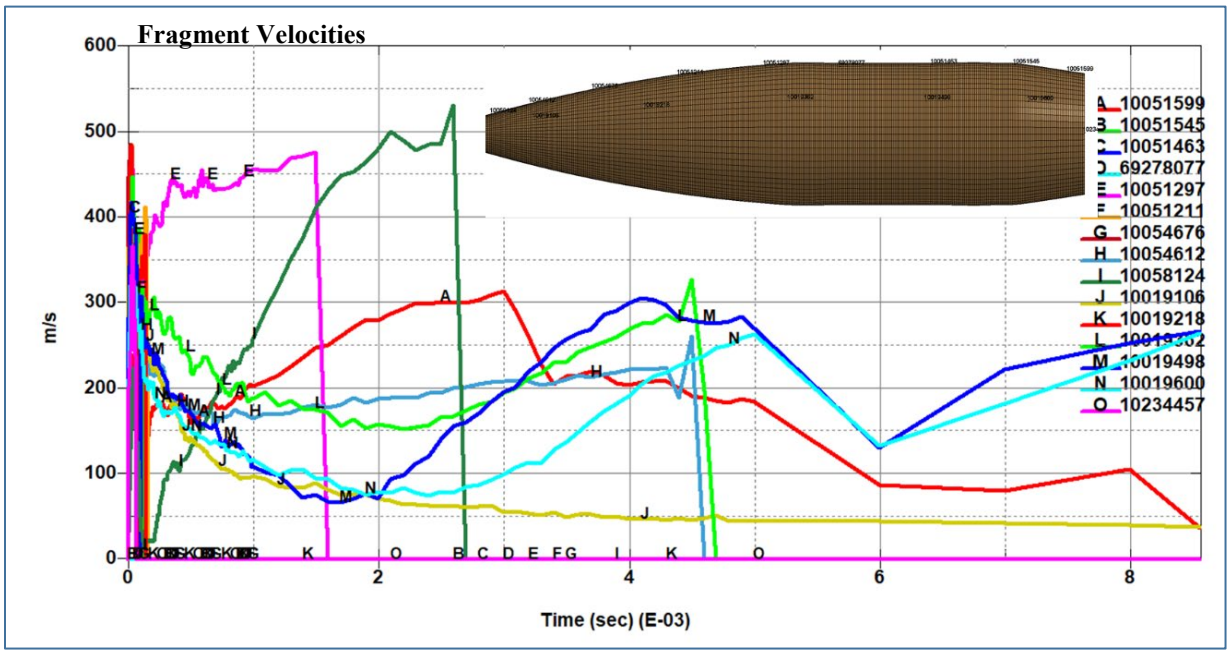

Figure11: Fragment velocity: Buried face Laid HE

Fragments travels from 0.2 meters to over 8 meters for surface laid HE. Absence of soil resistance results in significantly higher fragment travel for surface laid HE in contrast to the buried HE where in fragment are scattered within 1.5 meters. Fragment travel are captured in figure 12 and figure 13 for surface laid HE and buried HE respectively.

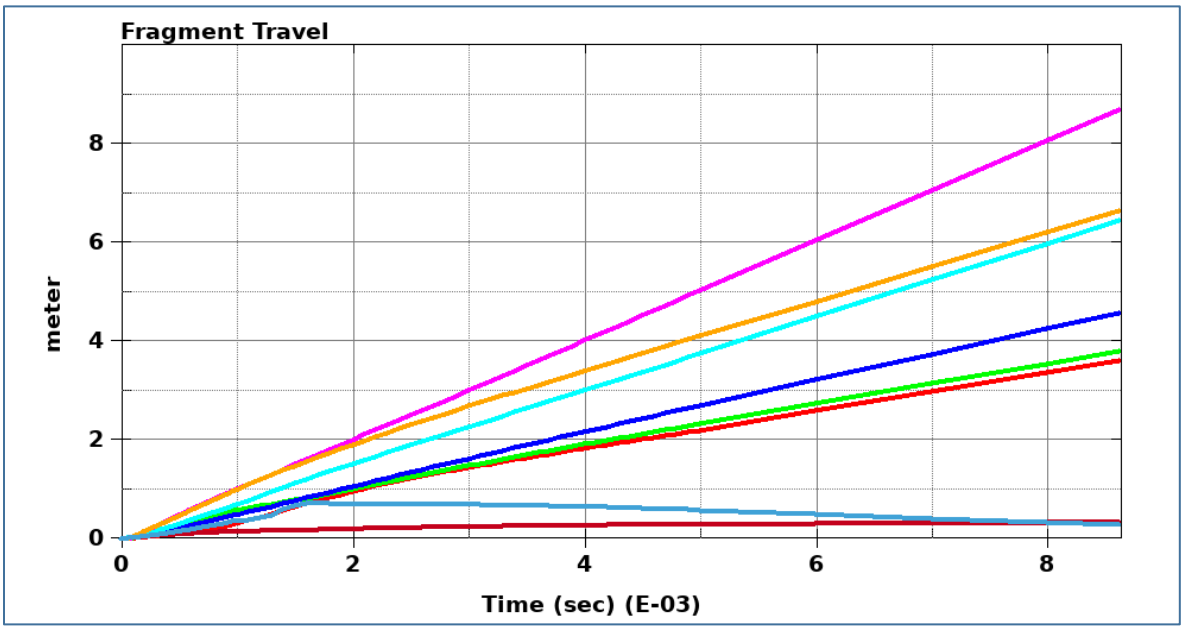

Figure 12: Fragment travel – Surface Laid HE

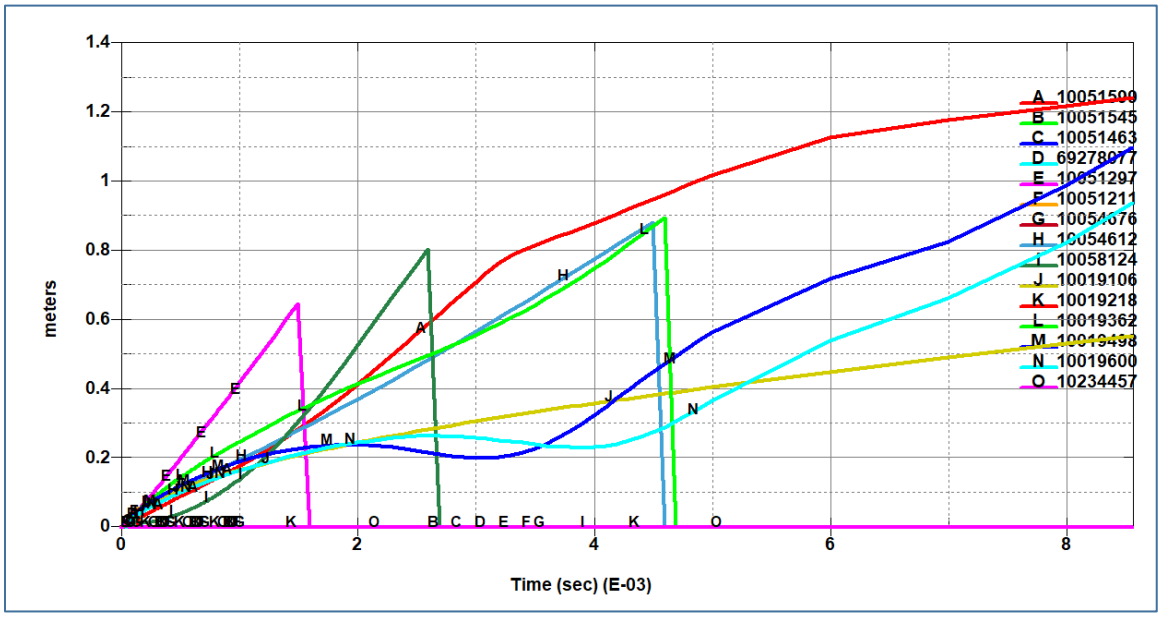

Figure 13: Fragment travel - Buried HE

4.3 Projectile casing stresses and strains

As mentioned earlier in section 4.1, expanding volume generates very high stresses and strains on the inner surface of the projectile casing, resulting in gradual rupture of the casings and fragments formed. Figure 14 shows that projectile casing volume expands for about 100 microseconds, before starts to rupture.

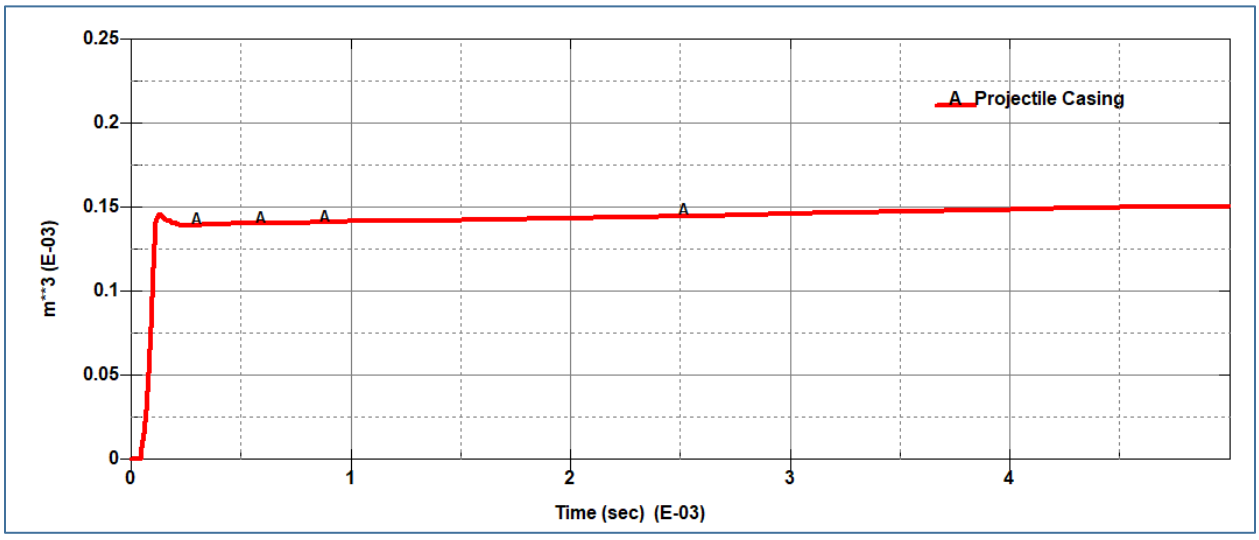

Figure 14: Projectile Casing – volume expansion

Stresses and strains generated on the Lagrange projectile casing captured in figure 15 and figure 16. Also in the figures 15 and 16, eroded elements and retained elements (fragments) are marked. Once the elements failed and eroded, stresses and strains reach zero for eroded elements. These failed and eroded elements constitutes as lost mass. The elements which become fragments continue to carry the mass, momentum and energy that are shown as curves with varying stresses and effective plastic strains.

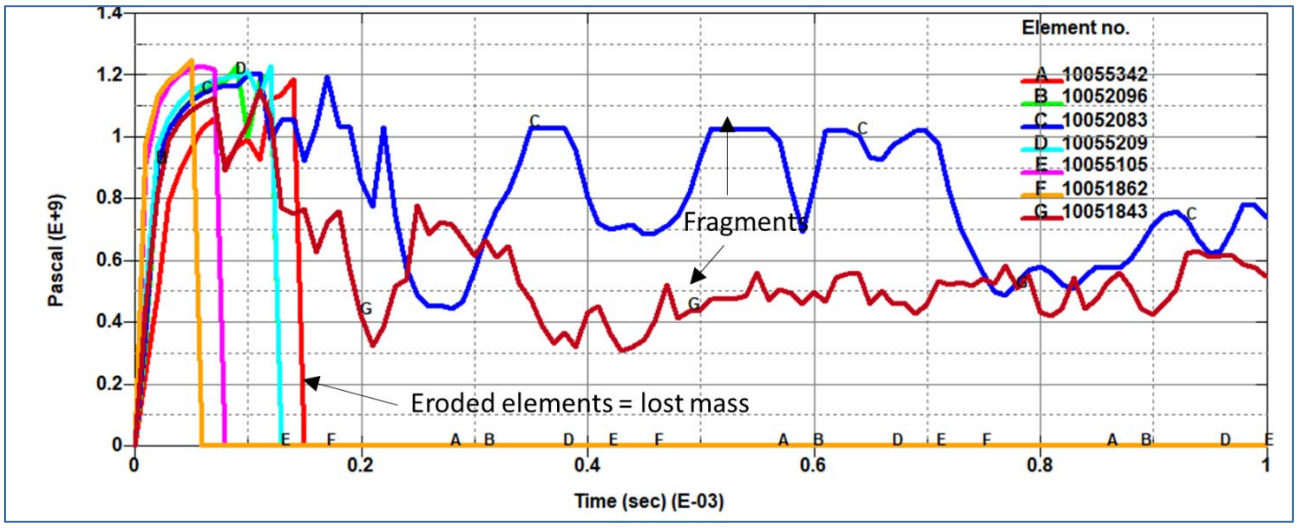

Figure 15: Projectile casing – Von Mises Stresses

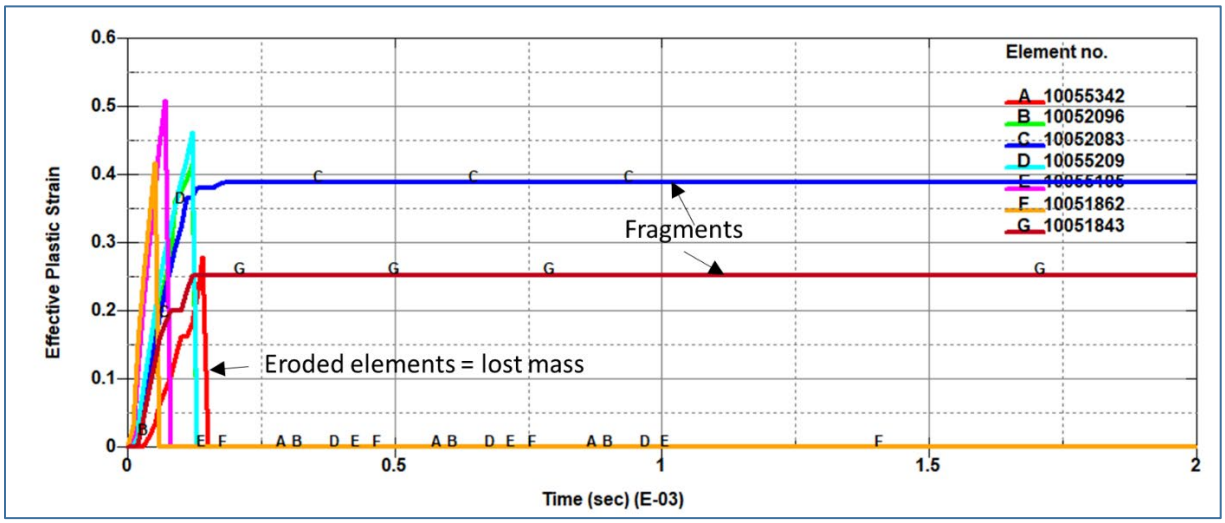

Figure 16: Projectile casing – Effective Plastic Strains

4.4 Energies

Internal energies of Lagrangian projectile casing for ALE, surface laid HE and buried HE are shown in figure 17 and figure 19 and kinetic energies are in figure 18 and figure 20. Internal energies of projectile casing for surface laid HE and buried HE with adaptive SPH are close to each other, whereas for ALE projectile casing internal energy is twice that. Kinetic energies of ALE and buried HE are similar, but the surface laid HE shows twice that of ALE and buried HE with adaptive SPH casing. In case of surface laid HE, absence of soil results in higher kinetic energies whereas in case of buried HE presence of soil has a damping effect which results in lower kinetic energy. In all the three cases energy component from lost mass due to rupture and erosion is not accounted

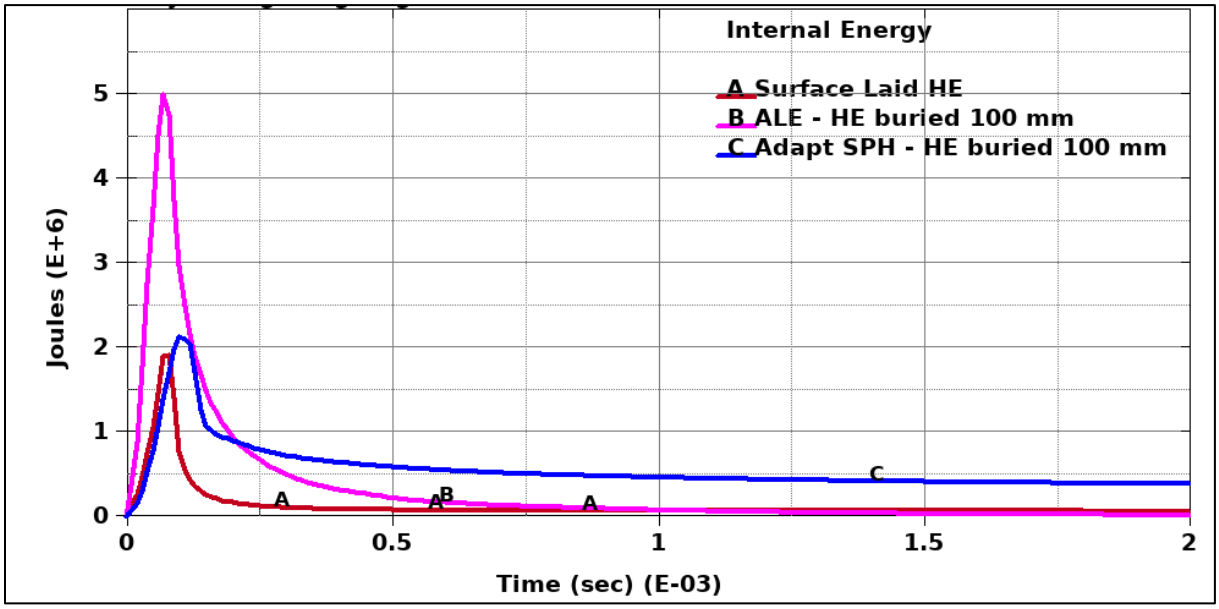

Figure 17: Internal Energy – Lagrange Projectile Casing

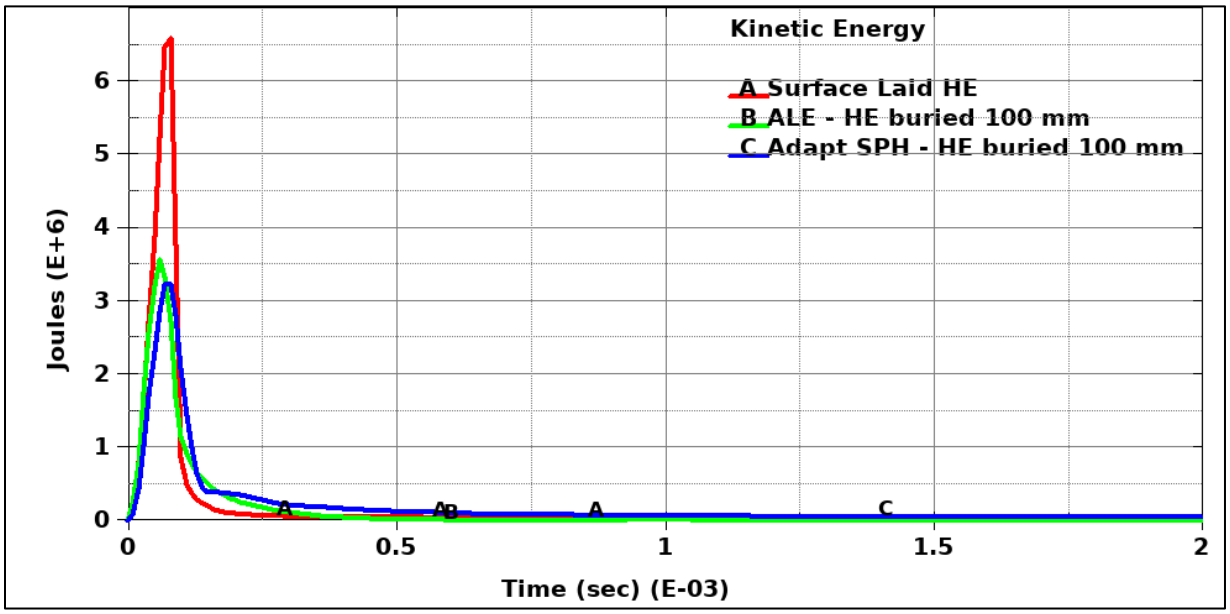

Figure 18: Kinetic Energy – Lagrange Projectile Casing

When the projectile casing was modeled with adaptive SPH, lost mass due to erosion will be retained and converted into SPH particles and carries material properties. Internal energies and kinetic energies of the adaptive SPH projectile casing are presented in figures 17, 18, 19 and 20. It is obvious to expect higher kinetic energy for fragmented particles in case of surface laid HE than that of the buried HE and the curves in figure 20 shows that. Conversely the internal energies are in opposite trend i.e., higher for buried HE and lower for surface laid as in figure 19.

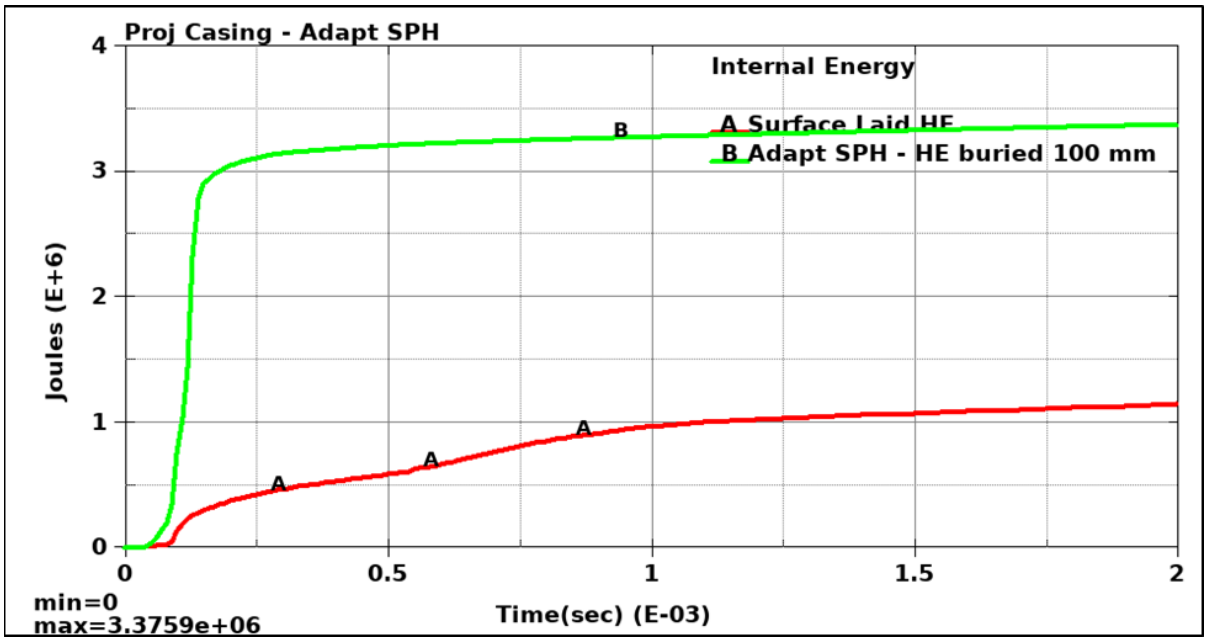

Figure 19: Internal Energy – Adapt SPH Projectile Casing

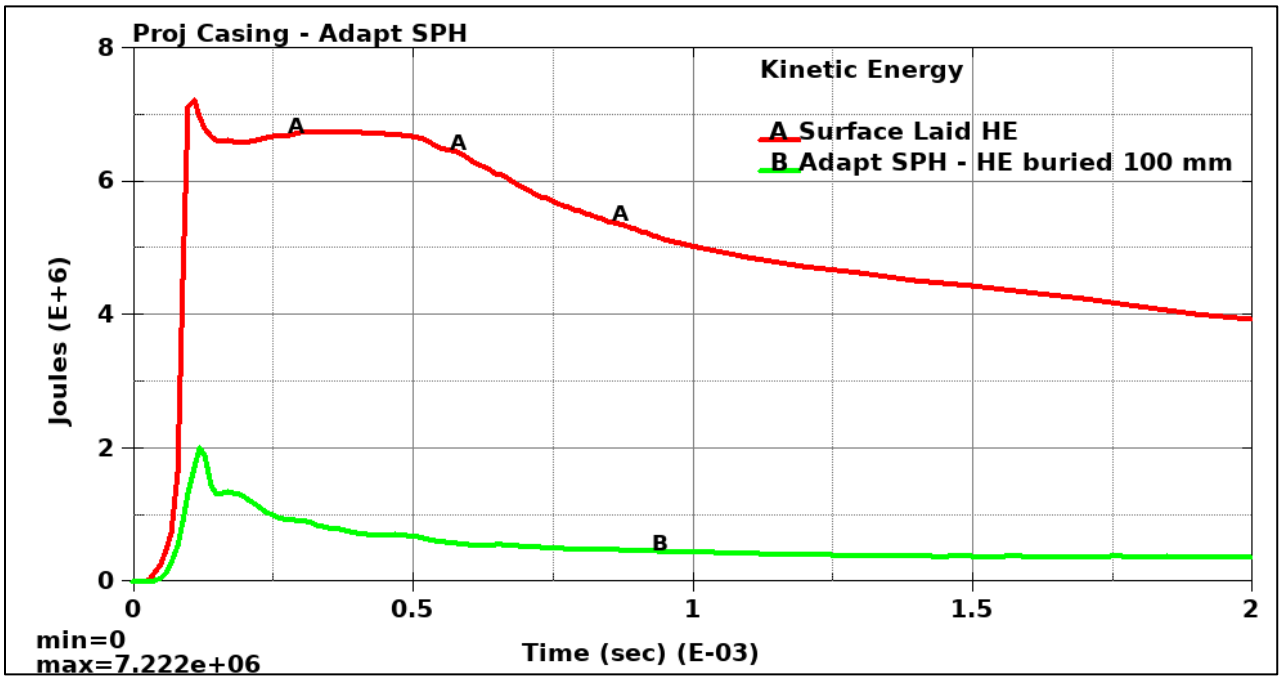

Figure 20: Kinetic Energy – Adapt SPH Projectile Casing

Table 2 summarizes the internal and kinetic energies plotted in figure 19 and 20.

Table 2: Internal and Kinetic Energies of projectile casing

Projectile Casing	High Explosive Location	Internal Energy (Joules)	Kinetic Energy (Joules)
Lagrange	Surface Laid	1.90E+06	6.50E+06
Lagrange	Buried 100mm	2.12E+06	3.20E+06
ALE	Buried 100 mm	4.99E+06	3.60E+06
With adapt SPH	Surface Laid	1.30E+06	7.20E+06
With adapt SPH	Buried 100mm	3.40E+06	2.00E+06

4.4 Coupled to GH

Fragments coupling to GVSC GH structure are shown for buried HE and surface laid HE in figures 21 and figure 22. Picture clearly shows how the fragments differ significantly for HE locations whether surface laid or buried deep in soil. Number of fragments, velocities and distance travelled are uniquely different

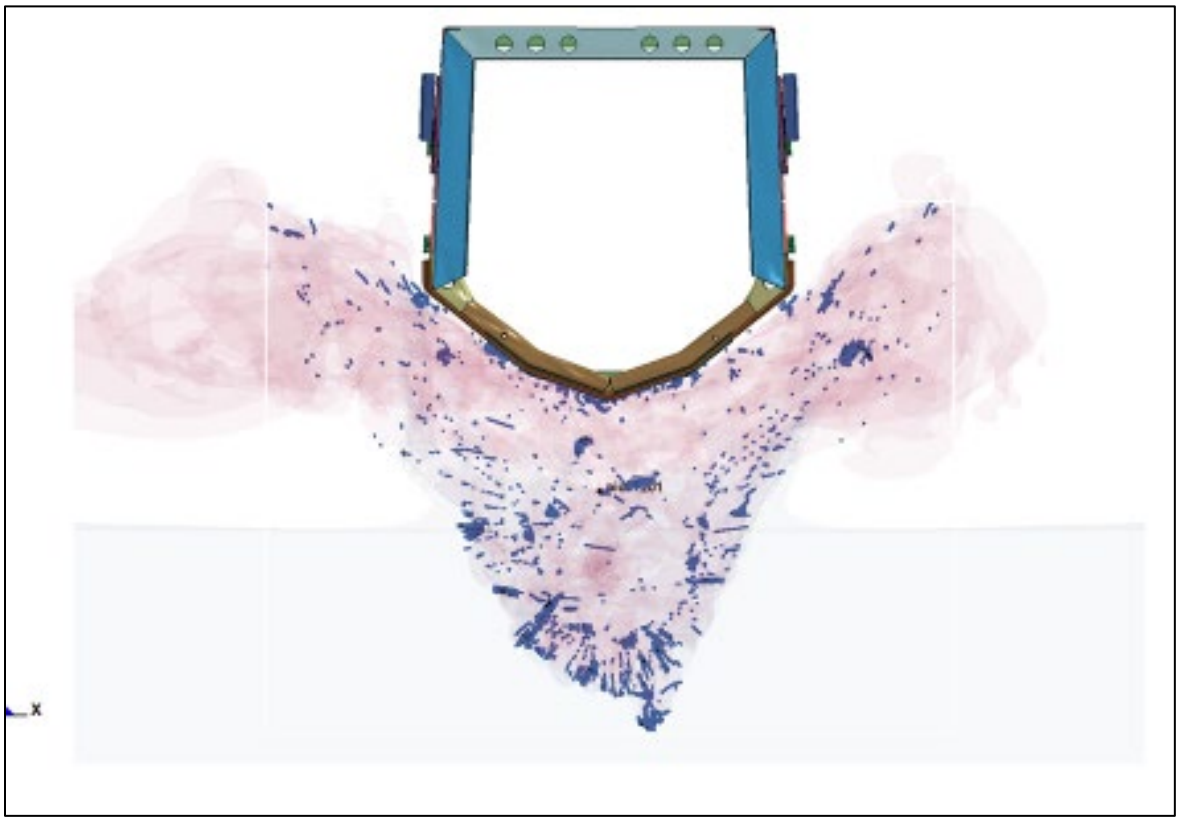

Figure 21: Fragments coupled GH – Buried HE

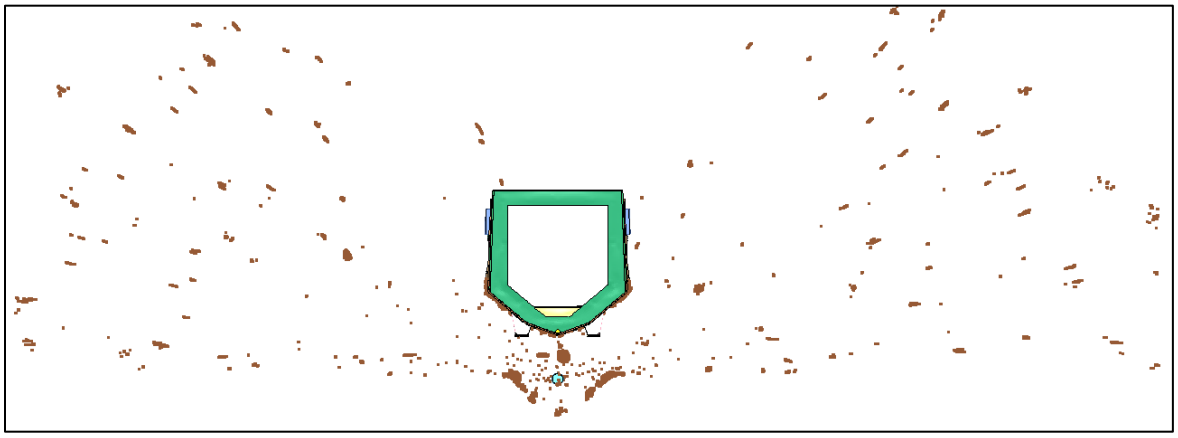

Figure 22: Fragments coupled GH – Surface Laid HE

Impulse is calculated by multiplying the global vertical velocity of the GH structure to the mass. Global velocities of the GH structure is shown in figure 23 for all the three cases, surface laid, ALE and buried HE. Surface laid HE has the least global velocities compared to that of ALE and buried HE. ALE and buried HE projectile results in higher global structural velocities augmented by the soil pressure and ejecta, whereas in case of surface laid HE it is purely the projectile

casing and explosive pressure. Lower global vertical velocity will result in lower total impulse for surface laid HE.

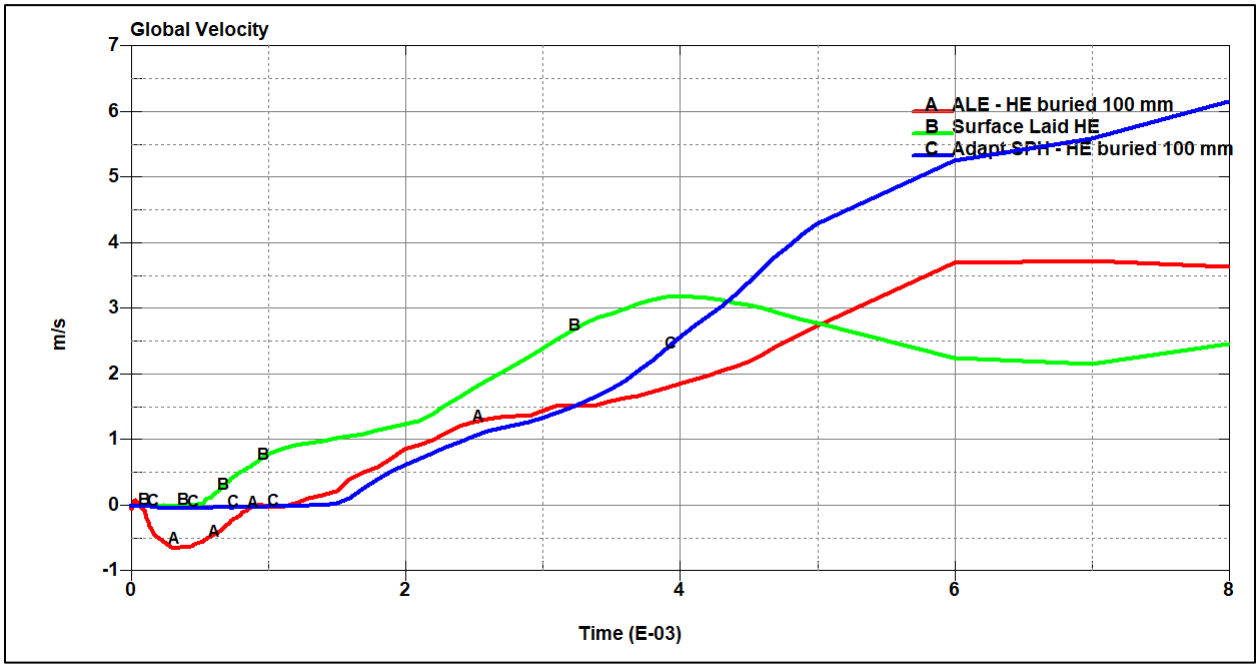

Figure 23: Global velocities of GH structure

5.0 Conclusion

Numerical simulation of fragmentation process of OF-540 projectile was successfully carried out by positioning the OF-540 projectile on the soil surface and buried 100 mm deep inside the soil. Numerical simulation was carried out first with projectile buried in soil without coupling to any structure to establish the numerical stability and fragmentation process. Having established the confidence in simulating the fragmentation process, projectile was coupled to the GVSC developed GH structure. Projectile casing was modeled with Eulerian, Lagrangian methods shows loss of mass due to rupture and element erosion. This resulted in inaccurate conservation of mass, momentum and energy as measured by the global velocities of the structure. To overcome the loss of mass, projectile casing was modeled as an adaptive SPH particles and simulated for surface laid and buried deep inside soil initial boundary conditions. Simulation shows that, this method converts the failed Lagrange elements into SPH particles and these particles carries the mass, momentum and conserves the energy. The overall simulation attempted to show, the detailed analysis of fragmentation process, lost mass, stresses & strains, fragment velocities & displacements and how the explosive energy transforms into internal and kinetic energies of projectile casing and its effects on the GH structural response. Simulation also shows that loss of projectile casing mass is not element sensitive. In summary

- Surface laid HE with adaptive SPH projectile casing produces
    - *more fragments, less impulse load on the GH structure*
- ALE with Eulerian projectile casing produces

  - *less fragments, higher impulse load on the GH structure*
  - *loss of projectile casing mass due to erosion*
- ALE with adaptive SPH projectile casing
  - *has the highest impulse load on the GH structure*
  - *failed projectile casing converted into SPH particles – No lost mass*

Element deletion from computation due to erosion in Lagrange and Euler methods, leads us to explore different meshless methods such as DEM, SPH or SPG. Although these meshless methods are computational intensive and takes up too much memory, but they provide deep insight into the physical phenomenon that happens inside the projectile which is extremely difficult to capture by physical testing. Also from a physical test point, it is challenging to count all the fragments from the failed projectiles as they are scattered all around the field. Only visible fragments can be counted. Analyzed method here in this research provides valuable information and better understanding of the fragmentation process, damage mechanisms and its effect on structure.

Acknowledgements

Terminologies

Surface Laid HE = Projectile laid on soil surface – Projectile casing as Lagrange with adaptive SPH particles

ALE = Projectile buried 100 mm deep inside soil - Projectile casing as Eulerian

Buried HE = Projectile buried 100 mm deep inside soil – Projectile casing as Lagrange with adaptive SPH particles

Abbreviations

ALE – Arbitrary Lagrange in Euler

ALE FSI – Arbitrary Lagrange in Euler Fluid Structure Interaction

CLIS – Constrained Lagrange in Solid

CCDC – Combat Capability Development Center

DEM – Discrete Element Method

GH – Generic Hull

GVSC – Ground Vehicle System Center

HE – High Explosive

IE – Internal Energy

IED – Improvised Explosive Device

JWL – Jones-Wilkins-Lee

KE – Kinetic Energy

SPH – Smooth Particle dynamics

SPG – Smooth Particle Galerkin

RHA – Rolled Homogeneous Armor

References

[1] Daniel Dooge, D., Ramesh Dwarampudi, R., Schaffner, G., Miller, A., Thyagarajan, R., Vunnam, M., and Babu, V., Evolution of Occupant Survivability Simulation Framework Using FEM-SPH Coupling, 2011 NDIA Ground Vehicle Systems Engineering and Technology Symposium (GVSETS), Dearborn, MI, 9-11 August 2011, DTIC Report # ADA 547566.

[2] UGRČIĆ,M.: Numerical simulation of the Fragmentation process of high explosive projectiles, Scientific Technical Review, ISSN 1820-0206, 2013, Vol.63, No.2, pp. 47-57.

[3] GRADY,D.E.: Investigation of explosively driven fragmentation of metals-two-dimensional fracture and fragmentation of metal shells, Progress Report II, US. Department of Energy, Lawrence Livermore National Laboratory, UCRL-CR-152264, B522033, 2003.

[4] MOTT,N.F., LINFOOT,E.H.: A theory of fragmentation, British Ministry of Supply Report, AC 3348, 1943.

[5] GOLD,V.M., BAKER,E.L., POULOS,W.J., FUCHS,B.E.: PAFRAG modeling of explosive fragmentation munitions performance, International Journal of Impact Engineering, Elsevier, 33, 2006, pp. 294–304.

[6] Mott N., Linfoot E. (2006) A Theory of Fragmentation. In: Fragmentation of Rings and Shells. Shock Wave and High Pressure Phenomena. Springer, Berlin, Heidelberg

[7] D. E. Grady, Fragmentation of Rings and Shells (Springer-Verlag, Berlin, 2006).

[8] P. Rosin and E. Rammler, J. Inst. Fuel **7**, 29 (1933)

[9] Halquist, J.O., LS-DYNA keyword user's manual version 971, Livermore Software Technology Corporation, Livermore, CA, 2007.

[10] Sensitivity of Particle Size in Discrete Element Method to Particle Gas Method (DEM_PGM) Coupling in Underbody Blast Simulations, V Babu, K Kulkarni, S Kankanalapalli, R Thyagarajan - 2016

[11] Johnson, G.R. and W.H. Cook, ‘‘A constitutive model and data for metals subjected to large strains, high strain rates and high temperatures,’’ Proceedings 7th International Symposium on Ballistics, The Ha April 19–21, The Netherlands, 1983.